Nanoscience and Nanometrology
2025; 9(1): 11-19
http://www.sciencepublishinggroup.com/j/nsnm
doi: 10.11648/j.nsnm.20250901.12

Geometric Influence on Optical Bistability and Local Field Enhancement in Core-Shell Nanocomposites

Shewa Getachew Mamo[1, *], Eyasu Tadese Muda[2]

[1]Department of Physics, Wolkite University, Welkite, Ethiopia
[2]Department of Physics, Dilla University, Dilla, Ethiopia

Email address:
shewa.getachew@wku.edu.et (Shewa Getachew), joshtadese@gmail.com (Eyasu Tadese)
[*]Corresponding author

To cite this article:
Shewa Getachew Mamo, Eyasu Tadese Muda. (2025). Geometric Influence on Optical Bistability and Local Field Enhancement in Core-Shell Nanocomposites. *Nanoscience and Nanometrology, 9*(1), 11-19. https://doi.org/10.11648/j.nsnm.20250901.12

Received: 30 May 2025; **Accepted:** 25 June 2025; **Published:** 25 September 2025

Abstract: This work investigates the role of geometric shape in tuning the optical bistability (OB) and local field enhancement factor (LFEF) of metal-coated dielectric core-shell (CS) nanoinclusions embedded in nonlinear dielectric host matrices. Through quasi-static analysis and Drude-based modeling, the study reveals that spherical and cylindrical nanoinclusions exhibit distinct OB thresholds and LFEF behaviors depending on their radii, dielectric environments, and shape-induced plasmonic resonances. Spherical CS nanostructures display stronger OB responses and field confinement at lower thresholds than their cylindrical counterparts. Results show that increasing host permittivity significantly widens the OB region, while reducing nanoinclusion size enhances optical nonlinearity. This investigation underscores the sensitivity of nonlinear optical responses to geometry, shell thickness, and host environment, providing valuable insights for designing tunable photonic components, including switches and optical memory devices.

Keywords: Enhancement Factor, Optical Bistability, Host Matrix, Nanocomposites, Core-shell

1. Introduction

Over the last three decades, significant advancements have been made in the study of the optical properties of nanoparticles, particularly core-shell (CS) nanocomposites (NCs), which have emerged as one of the most widely employed nanostructures across various scientific and technological domains [1]. A multitude of studies have established that the optical behavior of CS NCs is highly sensitive to numerous parameters, including the particle size, metallic composition, dielectric environment, and the spatial configuration of the core-shell architecture [2–5].

Among these influencing parameters, the shape of CS nanostructures plays a critical role in determining their surface plasmon resonances (SPRs). While the size and embedding media have traditionally been regarded as primary factors, recent works have demonstrated that even slight alterations in the geometry of the nanocomposites can significantly modify their SPR characteristics [6–8]. This geometric sensitivity offers a powerful mechanism to engineer the plasmonic and optical responses of nanostructures, thereby extending their applicability in tailored photonic devices.

Spheroidal CS nanocomposites, characterized by either prolate or oblate ellipsoidal shapes, have garnered special interest due to their capability to extend optical tunability over the visible to infrared spectral ranges. These structures, typically comprising a dielectric core enveloped by a metallic shell, support plasmon resonances that are highly adjustable through modifications in shape and size [9–11].

The synergy between plasmonic metal shells and dielectric cores forms the foundation of unique optical behaviors observed in bimetallic CS nanostructures. Enhanced coupling between incident electric fields and collective electron oscillations within the shell leads to pronounced SPR effects. These are further influenced by the interplay between the shell plasmons and the core dielectric properties [12–15].

Experimental and theoretical investigations have shown that CS nanostructures with noble metal shells (e.g., Au, Ag) and dielectric cores (e.g., SiO_2) exhibit superior performance in applications such as Surface-Enhanced Raman Scattering (SERS), where the enhancement of the electromagnetic field is crucial [16–21]. The location and intensity of the SPR bands in such systems are directly governed by parameters including shell thickness, core diameter, and surface morphology [22–28].

Recent advancements have also underscored the biomedical and optoelectronic significance of nanoparticles such as Ag and ZnO due to their excellent antimicrobial activity and favorable optical properties. These properties make them desirable candidates in pharmaceutical formulations, biosensing platforms, and diagnostic imaging tools [29–36]. Additionally, SiO_2 coatings on quantum dots (QDs) significantly improve their optical stability and biocompatibility, allowing for applications in long-term cellular imaging and targeted drug delivery [37–39].

In optoelectronics, materials like ZnTe play an indispensable role due to their doping versatility and high quantum efficiency. ZnTe has been widely used in devices ranging from laser diodes and blue LEDs to solar cells and terahertz generators. In particular, its integration with CdTe enhances photovoltaic efficiency by suppressing undesirable interfacial phenomena [40–47].

Several experimental and computational studies have investigated the optical response of core-shell nanocrystals including combinations such as SiO_2@Au [48], Ag@SiO_2 [49] and CdSe@Ag [50]. However, a comprehensive understanding of how geometry specifically spherical versus cylindrical inclusion shapes affects optical bistability (OB) and local field enhancement factor (LFEF) in nonlinear dielectric environments remains limited.

This study addresses that gap by presenting a detailed theoretical and numerical investigation of LFEF and OB in metal-coated dielectric CS nanoinclusions with different geometries embedded in active host matrices. The analysis incorporates the Laplace equation for potential distribution, Drude-Sommerfeld theory for the metallic response, and Kerr-type nonlinearities in the dielectric core. Our findings show that geometry, CS radii, and host permittivity collectively govern the nonlinear optical behavior, offering insights essential for the rational design of nanophotonic devices.

2. Simulations and Theoretical Basis

Our study focused on a type of nanocomposite known as spherical and cylindrical metal-coated dielectrics (NCs). These NCs consist of a dielectric core with radius r_1 and a dielectric function denoted by ε_d. The DF of the shell surrounding the core, represented by ε_m, varies with the applied electric field and has a radius of r_2. The whole nanocomposite is enclosed by a dielectric matrix composed of dielectric material with a dielectric function ε_h. The nanocomposite is subsequently exposed to incoming electromagnetic radiation [10, 14]. Different dielectric functions for the host matrices were studied in order to study the impact of geometric shape, core-shell radii, and various host matrices on optical characteristics. In this study, we looked at each of the two geometric shapes separately to better understand their impacts.

2.1. *Electric Potential Distribution in Cylindrical Core-shell NIs*

Through the application of boundary condition requirements and the solution of the Laplace equations for spherical $CS\ NIs$, the electric potential distributions in the core, shell, and store matrices was determined. Look at the parts of the CS nanocomposite materials where the dielectric core (DC) has a radius r_1 and the $DF\ \varepsilon_d$. The $DF\ \varepsilon_m$ and radius r_2 (with $r_1 < r_2$) produce the shell. The $DF\ \varepsilon_h$ describes the host material. The distribution of the electric potential in the host matrix, metallic shell, and DC can be explained by three distinct functions: ϕ_d for the host matrix, ϕ_m for the metal shell, and ϕ_h for the DC. According to [16–18], these functions are generated by the equation.

$$\begin{aligned}
\phi_d &= -E_h A r \cos\theta, && r \le r_1 \\
\phi_m &= -E_h \left(Br - \frac{C}{r^2}\right)\cos\theta, && r_1 \le r \le r_2 \\
\phi_h &= -E_h \left(r - \frac{D}{r^2}\right)\cos\theta, && r \ge r_2
\end{aligned}$$

The spherical coordinates of the observation point are represented by r and θ, whilst the applied electric field is represented by E_h. It corresponds with the vector E_h-axis. Because they are not provided, the values of the coefficients A, B, C, and D must be determined using the continuity equations for the vectors of displacement and electricity potential at the boundaries between the shell-host matrix and CS boundaries. In a CS nanocomposite materials electrical potential is continuous at the boundary between the dielectric core (DC) and the metallic shell. This method is based on the idea that since the electric potential along the interface cannot change abruptly, the potential values of the metallic (shell) and dielectric (core) portions must be comparable at the contact. The description for this condition is as follows:

$$\phi_d = \phi_m, \qquad r = r_1 \tag{1}$$
$$\phi_m = \phi_h, \qquad r = r_2 \tag{2}$$

The continuity of the displaced vector, which is connected to the electric field, must also be preserved at the contact. The situation can be described as follows:

$$\varepsilon_d \frac{\partial \phi_d}{\partial r} = \varepsilon_m \frac{\partial \phi_m}{\partial r}, \qquad r = r_1 \tag{3}$$
$$\varepsilon_m \frac{\partial \phi_m}{\partial r} = \varepsilon_h \frac{\partial \phi_h}{\partial r}, \qquad r = r_2 \tag{4}$$

whose dielectric constants are represented by the symbols ϵ_d, ϵ_m, and ϵ_h for the metal shell, dielectric host, and DC. Equations (2), (3), and (4) can be solved concurrently to provide the values of the following unknown coefficients:

$$A = \frac{9\epsilon_h \epsilon_m}{2p\eta} \tag{5}$$

$$B = \frac{3\epsilon_h(\epsilon_d + \epsilon_m)}{2p\eta} \tag{6}$$

$$C = \frac{3\varepsilon_h(\varepsilon_d - \varepsilon_m)}{2p\eta} r_1^3 \tag{7}$$

$$D = \left(1 - 3\varepsilon_h \frac{\varepsilon_m(3-p) + \varepsilon_d p}{2p\eta}\right) r_2^3 \tag{8}$$

According to $p = 1 - \left(\frac{r_1}{r_2}\right)^3$, In the inclusion, represents the metal volume fraction,

$$\eta = \epsilon_m^2 + q\epsilon_m + \epsilon_d \epsilon_h \tag{9}$$

$$q = \left(\frac{3}{2p} - 1\right)\epsilon_d + \left(\frac{3}{p} - 1\right)\epsilon_d \tag{10}$$

The Drude-Sommerfeld methodology provides a simple yet effective way to study the electrical and optical properties of electrons in metals, providing a theoretical basis for understanding their behavior. This model makes it simple to explain the metal's DF (ε_m), which describes the material's reaction to an external electric field and influences its optical properties. According to the Drude-Sommerfeld method, [10, 11] gives the metal's DF (ε_m):

$$\epsilon_m = \epsilon_\infty - \frac{1}{z(z + iz)} \tag{11}$$

Here, the effect of bound electrons on the polarization ability is represented by ε_∞. The variable z displays the ratio of the incident energy frequencies (ω) to the bulk plasma frequency (ω_p), and γ displays the ratio of the charge damping constant (ν) to the frequency of plasma (ω_p). Additionally, the real and imaginary components of ε_m can be expressed as

$$\varepsilon_m = \varepsilon_m' + i\varepsilon_m'' \tag{12}$$

Where,

$$\epsilon_m' = \epsilon_\infty' - \frac{1}{z^2 + \gamma^2}, \qquad \epsilon_m'' = \epsilon_\infty'' + \frac{\gamma}{z(z^2 + \gamma^2)}$$

2.2. LFEF of CS Nanoinclusions

The quasi-static approach ensures that the electric field E_0, which should be directed across the z-axis, is uniform. The following is a description of the local energy found in the dielectric core E_d of the spherical nanoparticles using the relation $E = -\nabla\Phi$ [40]:

$$E_d = -\nabla\Phi = AE_h \tag{13}$$

Assume that equation (5) defines the complex function A. The term $LFEF$ refers to the actual quantity $|A|^2$. The $LFEF$ in the core can be found by squaring and rearranging equation (12) and then replacing it into equation (5).

$$|A|^2 = \frac{81\epsilon_h^2(\epsilon_m'^2 + \epsilon_m''^2)}{4p^2(\eta'^2 + \eta''^2)}. \tag{14}$$

where

$$\begin{aligned}
\eta' &= \epsilon_m'^2 - \epsilon_m''^2 + q'\epsilon_m' - q''\epsilon_m'' + \epsilon_d'\epsilon_h,\\
\eta'' &= 2\epsilon_d'\epsilon_m'' + q'\epsilon_m'' + q''\epsilon_m' + \epsilon_d''\epsilon_h,\\
\epsilon_h &= \epsilon_h' + i\epsilon_h'', \quad q = q' + iq'',\\
q' &= \left(\frac{3}{2p} - 1\right)\epsilon_d + \left(\frac{3}{p} - 1\right)\epsilon_h',\\
q'' &= -\left(\frac{3}{p} - 1\right)\epsilon_h''.
\end{aligned} \tag{15}$$

2.3. IOB in Metal-dielectric Nanocomposite Analytically

We now analyze a spherical dielectric particle with radius r_1, surrounded by a metal enclosure with radius r_2. The core is composed of a nonlinear dielectric material of the Kerr type, which is defined by a nonlinear DF:

$$\epsilon_d = \epsilon_d' + i\epsilon_d'' + \chi|E|^2 \tag{16}$$

Here, ϵ_d' represents the real part of the DF, while ϵ_d'' corresponds to the imaginary part (*ImP*) of the DF of the core. χ denotes the nonlinear Kerr coefficient, which typically depends on the frequency of the electromagnetic field, and $|E|$ indicates the local field amplitude within the core.

By substituting equations (10) and (16) into equation (9), we can rewrite it as follows:

$$\begin{aligned}
\eta &= \epsilon_m^2 - \Pi\epsilon_m + \epsilon_h(\epsilon_d + \chi|E|^2),\\
\eta &= \eta_0 + \sigma\chi|E|^2,
\end{aligned} \tag{17}$$

where η_0 and α are constants.

$$\begin{aligned}
\eta_0 &= \epsilon_m^2 - \epsilon_m\Pi + \epsilon_h\epsilon_d,\\
\Pi &= \epsilon_h\left(\frac{3}{2p} - 1\right) + \left(\frac{3}{2p} - 1\right)\epsilon_d,\\
\sigma &= \epsilon_h\left(\frac{3}{2p} - 1\right) + \epsilon_d,\\
\eta &= \eta' + i\eta'', \quad \sigma = \sigma' + i\sigma'',\\
\epsilon_m &= \epsilon_m' + i\epsilon_m'', \quad \epsilon_h = \epsilon_h' + i\epsilon_h''
\end{aligned}$$

Now, by multiplying both sides of the equation in equation (13) by χ after squaring:

$$\chi|E|^2 = |A|^2\chi|E_h|^2. \tag{18}$$

By replacing the local field EF in equation (18), we obtain:

$$\chi|E|^2 = \frac{81}{4p^2}\left|\frac{\epsilon_m\epsilon_h}{\alpha}\right|^2 \frac{\chi|E_h|^2}{\left|\frac{\eta}{\sigma}\right|^2 + 2\mathrm{Re}\left(\frac{\eta}{\sigma}\right)\chi|E|^2 + |\chi|E|^2|^2} \tag{19}$$

By letting $\zeta = \chi|E|^2$ and $Y = \chi|E|$, we obtain the following cubic equation for ζ:

$$\zeta = \frac{81}{4p^2}\left|\frac{\epsilon_m\epsilon_h}{\sigma}\right|^2 \frac{Y}{b + a\zeta + \zeta^2}. \tag{20}$$

To compute the local field of the particle, we derive the cubic equation:

$$\zeta^3 + a\zeta^2 + b\zeta = \phi Y, \tag{21}$$

where

$$a = 2\mathrm{Re}\left(\frac{\eta}{\alpha}\right), b = \left|\frac{\eta}{\alpha}\right|^2,$$
$$\phi = \frac{81}{4p^2}\left|\frac{\epsilon_m\epsilon_h}{\sigma}\right|^2 \tag{22}$$

The equation (22) describes how the local field is influenced by the applied field, the dimensionless frequency z, the dielectric core, and other system parameters.

3. Numerical Results and Discussion

In this study, we investigated the enhancing factor and OB of $ZnTe@Ag$ CS nanostructures embedded in various surrounding matrices. The model considers a silver (Ag) shell with a dielectric core of $ZnTe$, analyzed for different host media [43, 44]. The parameters used in the numerical calculations are: $\varepsilon_\infty = 4.5$, plasma frequency $\omega_p = 1.6 \times 10^{16}$ rad/s, dimensionless frequency $z = 0.2$, and damping constant $\nu = 1.67 \times 10^{14}$ rad/s. Table 1 summarizes the physical constants used, based on values from references [10, 11].

Table 1. *Physical constants used in numerical computations.*

Constant	Value
ε_d	9.8
ε_h	2.5
ε_∞	4.5
γ	1.15×10^{-2}

Figure 1 displays the $LFEF$ as a function of the dimensionless frequency z for spherical and cylindrical nanocomposites, keeping the shell thickness fixed at $r_2 = 30\,$nm. The $LFEF$ exhibits two distinct resonance peaks for both shapes. Notably, the first resonance peak (at lower frequencies) shifts toward lower frequencies when transitioning from cylindrical to spherical nanostructures, while the second resonance peak shifts to higher frequencies. Moreover, the $LFEF$ magnitude of spherical nanocomposites is approximately 2.3 times greater than that of cylindrical ones at the same CS radii. This difference is attributed to the geometrical influence on plasmon hybridization modes, consistent with the quasi-static plasmon hybridization theory [45, 46, 48]. According to this theory, the plasmon resonances arise from coupling between sphere plasmons (outer shell surface) and cavity plasmons (inner shell surface), yielding symmetric (lower energy) and antisymmetric (higher energy) modes influenced by shell thickness and shape.

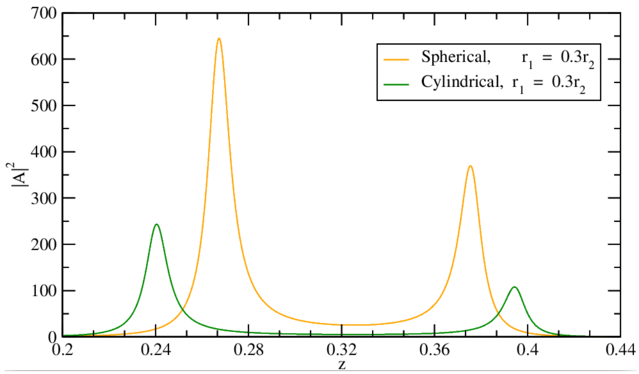

Figure 1. *Local field enhancement factor ($LFEF = |A|^2$*

The effect of varying the core-shell radii ratio r_1/r_2 on the $LFEF$ for spherical and cylindrical nanocomposites is shown in Figures 2(a) and 2(b), respectively. For spherical nanostructures (Figure 2(a)), increasing the core radius results in a blue shift of the first resonance peak (shift to higher frequencies or shorter wavelengths) and an increase in peak intensity. Conversely, the second resonance peak exhibits a slight red shift (to lower frequencies or longer wavelengths) with increasing core radius. This behavior reflects modifications in the localized electromagnetic field distribution within the core-shell structure, affecting how incident light couples to plasmon modes. Cylindrical nanocomposites (Figure 2(b)) show qualitatively similar trends, although the shifts and intensities differ due to geometry.

Figures 2(a) and (b) collectively reveal that as the ratio r_1/r_2 decreases, the first resonance peak shifts toward higher frequencies (blue shift), while the second peak shifts slightly toward lower frequencies (red shift). This indicates that reducing the core radius relative to the shell enhances the local electromagnetic field inside the nanostructure and tunes the resonance frequencies. Such tunability is valuable for designing nanocomposites with tailored optical properties.

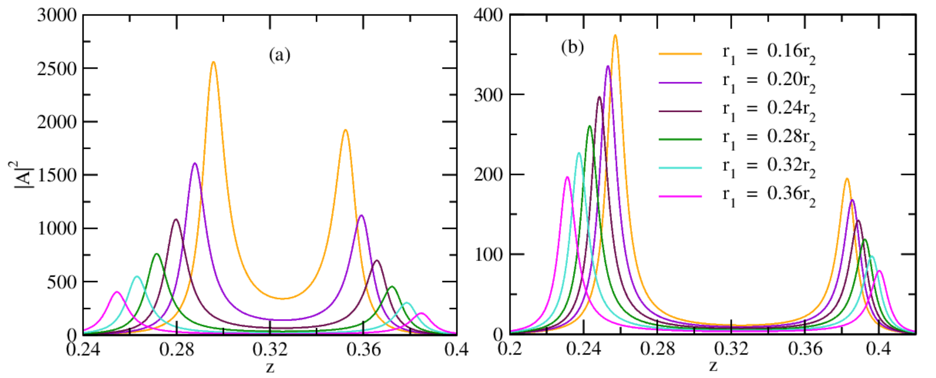

Figure 2. *Effect of core-shell radius ratio r_1/r_2 on $LFEF$ of (a) spherical and (b) cylindrical core-shell nanocomposites with host dielectric constant $\varepsilon_h = 2.5$.*

Figure 3 explores the influence of the host matrix dielectric constant ε_h on $LFEF$ for spherical and cylindrical nanocomposites at fixed radius ratio $r_1/r_2 = 0.22$. Increasing ε_h shifts both resonance peaks to different frequencies and increases the magnitude of $LFEF$. The results show a more pronounced enhancement for spherical nanocomposites, with the first peak $LFEF$ rising from about 90 for cylindrical structures to nearly 270 for spherical ones. This amplification arises because a higher host dielectric constant modifies the local field environment around the nanostructure, enhancing light-matter interaction [47].

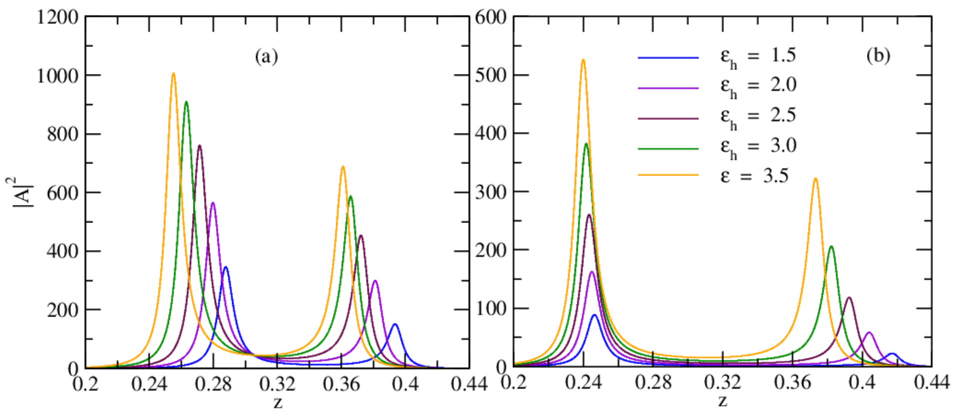

Figure 3. *Influence of host matrix dielectric constant ε_h on $LFEF$ of (a) spherical and (b) cylindrical core-shell nanocomposites with fixed radius ratio $r_1/r_2 = 0.22$.*

The geometric shape effect on $LFEF$ is further highlighted in Figure 4. When the dielectric constant of the core ε_d exceeds that of the host matrix ε_h, spherical nanocomposites show higher $LFEF$ compared to cylindrical ones. Conversely, for $\varepsilon_d < \varepsilon_h$, cylindrical nanocomposites yield larger $LFEF$. These findings suggest that for high $LFEF$, cylindrical nanocomposites are favorable when the core has a relatively low dielectric constant, whereas spherical structures dominate when the core dielectric is higher.

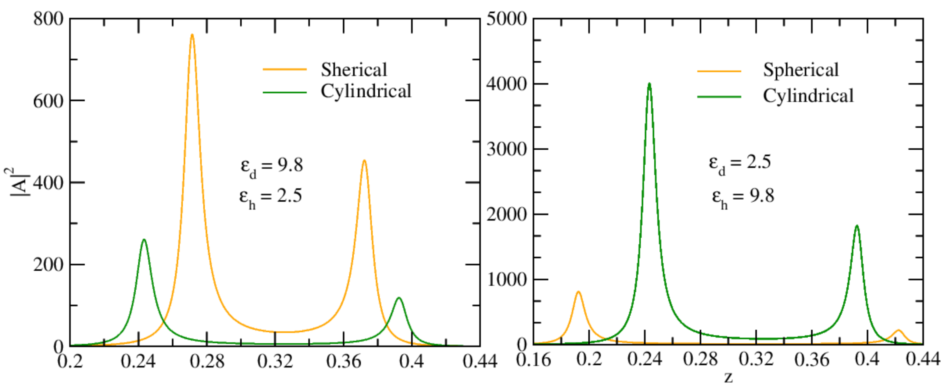

Figure 4. *Effect of core dielectric constant on $LFEF$ for (a) spherical and (b) cylindrical core-shell nanocomposites with radius ratio $r_1/r_2 = 0.22$.*

Figures 5(a) and 5(b) illustrate the effect of the core-to-shell radius ratio on the OB threshold for spherical and cylindrical nanoinclusions with $\varepsilon_h = 2.25$. We observe that the OB threshold increases as the ratio r_1/r_2 decreases, implying that stronger incident fields are required to induce bistability for smaller core radii. Spherical nanoinclusions exhibit a lower OB threshold compared to cylindrical ones, likely due to their higher symmetry and stronger field localization, which facilitate bistability at reduced applied fields.

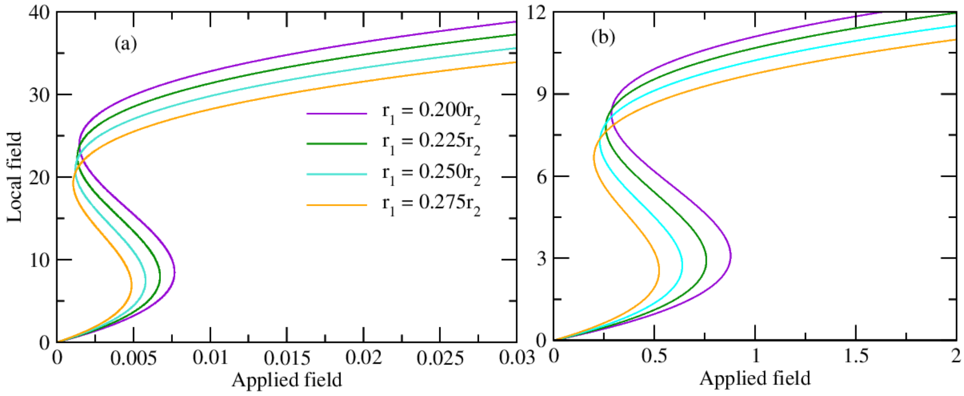

Figure 5. Effect of core-shell radius ratio r_1/r_2 on optical bistability (OB) of (a) spherical and (b) cylindrical core-shell nanoinclusions with $\varepsilon_h = 2.25$.

The influence of the host matrix dielectric constant on OB is presented in Figure 6 for fixed radius ratio $r_1/r_2 = 0.22$. Both the up and down switching intensities increase with increasing ε_h, broadening the OB hysteresis loop. This means that nanocomposites embedded in matrices with higher dielectric constants require stronger applied fields to switch states, but they also exhibit larger bistability ranges. Such control over OB characteristics via the host matrix can be exploited in optical switching and memory device design.

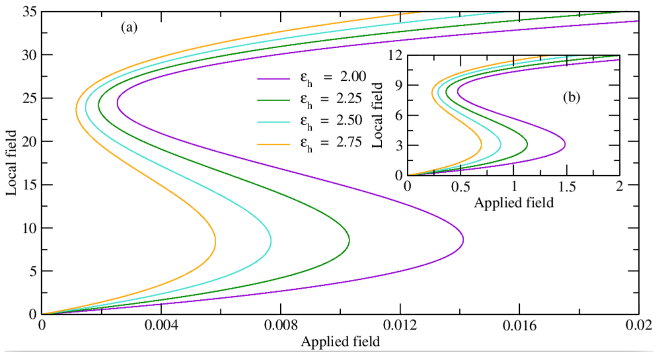

Figure 6. Effect of host matrix dielectric constant on optical bistability (OB) of (a) spherical and (b) cylindrical core-shell nanoinclusions with radius ratio $r_1/r_2 = 0.22$.

Finally, it is evident from Figure 5 that increasing the core-shell radius r_2 reduces the required applied field at the switching-up threshold, particularly for spherical nanocomposites. This implies that larger spherical nanostructures facilitate bistability at lower incident intensities, whereas cylindrical nanocomposites demand comparatively higher fields to achieve similar OB behavior.

4. Conclusion

This study investigated the effects of host matrix permittivity, CS radii, and geometric shape on the local field enhancement factor ($LFEF$) and OB of CS nanoinclusions. By solving the Laplace equation within the quasi-static approximation, expressions for the electric potential of the nanoinclusions were derived. Incorporating the Lorentz-Drude model and varying the CS radii, an analytical formula for the enhancement factor inside the core was established. The results reveal that, regardless of whether the CS radii were fixed or varied, the nanoinclusions exhibited two distinct enhancement factor peaks. Furthermore, increasing the host matrix permittivity ε_h led to a significant rise in the peak intensities of the enhancement factor. The shape of the nanoinclusions spherical versus cylindrical was found to strongly influence both the magnitude of the $LFEF$ and the optical bistability characteristics. Importantly, the enhancement factors and bistability thresholds could be effectively tuned by adjusting parameters such as the host matrix dielectric constant and the core-shell radii. These tunable optical properties highlight the potential practical applications of such nanoinclusions in areas including optical sensing, photonic circuits, logic devices, and optical memory technologies.

ORCID

0009-0005-8265-0115 (Shewa Getachew Mamo)
0009-0008-1393-8440 (Eyasu Tadese Muda)

Abbreviations

OB	Optical Bistability
LFEF	Local Field Enhancement Factor
CS	Core-shell
NCs	Nanocomposites
SPRs	Surface Plasmon Resonances
QDs	Quantum Dots
DC	Dielectric Core
DF	Dielectric Function

Authors Contributions

SGM and ETM conceptualized and created the model, carried out the analytical computations, and evaluated and interpreted the outcomes. The manuscript was prepared by SGM. After SG examined the findings, the final draft of the manuscript was approved by both authors.

Funding

The authors declare that no funds, grants, or other support were received during the preparation of this manuscript.

Data Availability Statement

There are either no related data for this manuscript or the data won't be deposited.

Conflicts of Interest

The authors have no relevant financial or non-financial interests to disclose.

References

[1] Bennink R S, Yoon Y-K, Boyd R W and Sipe J 1999 Nonlinear optical interactions in metals *Opt. Lett. 24* 1416-1418. https://doi.org/10.1364/OL.24.001416

[2] Arnold S, O'Keeffe T, Leung K, Folan L, Scalese T and Pluchino A 1990 The measurement of optical constants by attenuated total reflection *Appl. Opt. 29* 3473-3478. https://doi.org/10.1364/AO.29.003473

[3] Mahmudin L et al 2015 Optical properties of metal nanoparticles in glass matrix: A review *J. Mod. Phys. 6* 1071-1080.

[4] Stepanov A L 2016 *Glass Nanocomposites* (Amsterdam: Elsevier) pp 165-179.

[5] Brandl D W and Nordlander P 2007 Plasmon hybridization in nanoparticle dimers *J. Chem. Phys. 126* 144708. https://doi.org/10.1063/1.2719573

[6] Yu Y-Y, Chang S-S, Lee C-L and Wang C-C 1997 Gold nanoparticles formed by chemical reduction using sodium citrate *J. Phys. Chem. B 101* 6661-6664. https://doi.org/10.1021/jp9703177

[7] Yang W-H, Schatz G C and Van Duyne R P 1995 Discrete dipole approximation for calculating extinction and Raman intensities for small particles with arbitrary shapes *J. Chem. Phys. 103* 869-875. https://doi.org/10.1063/1.469098

[8] Lisiecki I, Billoudet F and Pileni M 1996 Gold nanoparticles formation studied by optical spectroscopy *J. Phys. Chem. 100* 4160-4166. https://doi.org/10.1021/jp953686t

[9] Lv W, Phelan P E, Swaminathan R, Otanicar T P and Taylor R A 2013 Evaluation of nanofluid-based direct absorption solar collector *J. Solar Energy Eng. 135* 021004. https://doi.org/10.1115/1.4024235

[10] Daneshfar N and Noormohamadi Z 2020 Optical and structural properties of nanoparticles synthesized by laser ablation in liquids *Appl. Phys. A 126* 55. https://doi.org/10.1007/s00339-019-3108-1

[11] Cui W, Li M, Dai Z, Meng Q and Zhu Y 2014 Surface plasmon resonance in metallic nanoshells *J. Chem. Phys. 140* 044109. https://doi.org/10.1063/1.4862296

[12] Encina E R, Prez M A and Coronado E A 2013 Nonlinear optical properties of gold nanorods in polymer matrices *J. Nanopart. Res. 15* 1688. https://doi.org/10.1007/s11051-013-1688-0

[13] Getachew S and Berga G 2024 Local field enhancement in core-shell nanostructures *Can. J. Phys.*

[14] Brett W, Byun B H and Kim J H 2013 Controlled synthesis of gold nanoparticles for biomedical applications *Gold Bulletin 46* 185-193. https://doi.org/10.1007/s13404-013-0101-2

[15] Getachew S and Aboma H 2024 Enhancing local field and optical bistability of cylindrical nanoinclusions within passive and active host matrices *Quantum Physics Letters 13*(1) 1-12. https://doi.org/10.18576/qpl/130101

[16] Yin H J *et al.* 2015 Multifunctional core-shell nanostructures for biomedical applications *Sci. Rep. 5* 14052. https://doi.org/10.1038/srep14052

[17] Hirpha T T, Bergaga G D, Ali B M and Gebre S S 2023 Tailoring the optical response of metal-based nanocomposites *Mater. Res. Express 10*(4) 045005. https://doi.org/10.1088/2053-1591/acc78a

[18] Getachew S 2024 Investigation of refractive index and group velocity of metal coated dielectric spherical nanocomposites within both passive and active dielectric cores *Iranian Journal of Physics Research 24*(3) 75-87 https://doi.org/10.47176/ijpr.24.3.51890

[19] Srnova-Vloufova I *et al.* 2000 SERS study of gold colloid-protein interactions *Langmuir 16* 9928-9935. https://doi.org/10.1021/la000732q

[20] Naseri T and Pour-Khavari F 2020 Localized surface plasmon resonance in gold nanoshells *Plasmonics 15* 907-914. https://doi.org/10.1007/s11468-019-01090-0

[21] Dab C, Thomas R and Andreas R 2018 Plasmon enhanced absorption in core-shell structures *RSC Adv. 8*(35) 19616-19626. https://doi.org/10.1039/C8RA03042F

[22] Shabaninezhad M and Ramakrishna G 2019 Plasmon hybridization and nonlinearities in nanoshells *J. Chem. Phys. 150* 144116. https://doi.org/10.1063/1.5091002

[23] Jackson J B, Westcott S L, Hirsch L R, West J L and Halas N J 2003 Surface-enhanced fluorescence on metal nanoshells *Appl. Phys. Lett. 82* 257-259. https://doi.org/10.1063/1.1535833

[24] Madamsetty V S, Mukherjee A and Mukherjee S 2019 Engineered nanocarriers in cancer therapy *Front. Pharmacol. 10* 1264. https://doi.org/10.3389/fphar.2019.01264

[25] Cholkar K, Hirani N D and Natarajan C 2017 Nanotechnology-based medical and biomedical imaging for diagnostics. In: Nanotechnology Applications for Tissue Engineering (Elsevier) pp 355-374.

[26] Yuwen L, Sun Y, Tan G, Xiu W, Zhang Y, Weng L, Teng Z and Wang L 2018 Plasmon-enhanced fluorescence with gold nanorods *Nanoscale 10* 16711-16720. https://doi.org/10.1039/C8NR04837C

[27] Crisan C M, Mocan T, Manolea M, Lasca L I, Tabaran F A and Mocan L 2021 Role of metal nanoparticles in photothermal therapy *Appl. Sci. 11* 1120. https://doi.org/10.3390/app11031120

[28] Jabeen S, Qureshi R, Munazir M, Maqsood M, Munir M, Shah S S H and Rahim B Z 2021 Optical characterization of gold nanoparticles *Mater. Res. Express 8* 092001. https://doi.org/10.1088/2053-1591/ac230b

[29] Muruganandham M *et al.* 2023 Gold nanostructures in optical sensors *Mater. Res. Express 10* 125006. https://doi.org/10.1088/2053-1591/ad10f6

[30] Yang P, Wang Y and Zhang L 2013 Plasmonic biosensing with nanoparticles *J. Nanosci. Nanotechnol. 13* 3011-3015. https://doi.org/10.1166/jnn.2013.7312

[31] Anderson B D, Wu W C and Tracy J B 2016 Synthesis and optical response of Au-Ag core-shells *Chem. Mater. 28*(14) 4945-4952. https://doi.org/10.1021/acs.chemmater.6b01653

[32] Bauer J 1977 Dielectric properties of nanostructured materials *Phys. Status Solidi A 39*(2) 411-418. https://doi.org/10.1002/pssa.2210390204

[33] Suthar D, Chuhadiya S, Sharma R and Dhaka M S 2022 Optical and electrical properties of nanostructures *Mater. Adv. 3* 8081-8107. https://doi.org/10.1039/D2MA00257E

[34] Atnaf T and Getachew S 2024 Investigation of optical properties of ZnTe@Ag core-shell spherical nanocomposites within various dielectric host matrices *Adv. Mater. 13*(4) 80-91. https://doi.org/10.11648/j.am.20241304.13

[35] Sun H, Liu J, Zhou C, Yang W, Liu H, Zhang X *et al.* 2021 Self-assembled nanostructures for photonic applications *ACS Appl. Mater. Interfaces 13* 16997-17005. https://doi.org/10.1021/acsami.1c03828

[36] Xia F, Yang F, Hu X, Zhang C and Zheng C 2020 Gold nanostructures in hybrid solar energy devices *ACS Omega 5* 21922-21928. https://doi.org/10.1021/acsomega.0c03022

[37] Limmer S J, Chou T P and Cao G 2003 Structural design of nanostructured materials for optoelectronics *J. Phys. Chem. B 107* 13313-13318. https://doi.org/10.1021/jp035056u

[38] Sun C 2018 Nonlinear optical effects in plasmonic nanocomposites *Plasmonics 13* 1671-1680. https://doi.org/10.1007/s11468-018-0704-5

[39] Liu L, Xu X, Ye Y, Ma Y, Liu Y, Lei J and Yin N 2012 Fabrication and optical characteristics of ZnO thin films *Thin Solid Films 526* 127-132. https://doi.org/10.1016/j.tsf.2012.03.046

[40] Beyene G, Sakata G, Senbeta T and Mesfin B 2020 Dielectric and plasmonic tuning in hybrid nanocomposites *AIMS Mater. Sci. 7* 705-719. https://doi.org/10.3934/matersci.2020.6.705

[41] Guenther R D 1990 *Modern Optics* (New York: Wiley) ISBN: 0-471-60538-7.

[42] Hau L V, Harris S E, Dutton Z and Behroozi C H 1999 Light speed reduction to 17 metres per second in an ultracold atomic gas *Nature 397* 594-598. https://doi.org/10.1038/17561

[43] Getachew S 2024 Effect of tunable dielectric core on optical bistability in cylindrical core-shell nanocomposites *Adv. Condens. Matter Phys. 2024* 9911970. https://doi.org/10.1155/2024/9911970

[44] Getachew S, Shewamare S, Diriba T and Berhanu G 2023 Geometric dependence of optical bistability in nanostructures *Int. J. Curr. Res. 15*(11) 24924-24929 https://doi.org/10.24941/ijcr.45824.11.2023

[45] Maier S A 2007 *Plasmonics: Fundamentals and Applications* (New York: Springer) ISBN: 978-0-387-37824-1.

[46] Pelton M and Bryant G 2013 *Introduction to Metal-Nanoparticle Plasmonics* (Hoboken: Wiley) ISBN: 978-1-118-02069-0.

[47] Aboma H 2025 Effect of tunable dielectric function of the core on optical bistability in small spherical metal-dielectric composite *Jefore Ethiop. J. Appl. Sci.* (Accepted)

[48] Prodan E, Radloff C, Halas N J and Nordlander P 2003 A hybridization model for the plasmon response of complex nanostructures *Science 302* 419-422. https://doi.org/10.1126/science.1089171

[49] Farokhnezhad M, Esmaeilzadeh M, Nourian M, Jalaeikhoo H, Rajaeinejad M, Iravani S and Majidzadeh-A K 2020 Gold nanostructures for biomedical applications *J. Phys. D: Appl. Phys. 53* 405401. https://doi.org/10.1088/1361-6463/ab93ce

[50] Shewamare S and Mal'nev V N 2012 Optical bistability in metallic nanocomposites *Phys. B: Condens. Matter 407* 4837-4841. https://doi.org/10.1016/j.physb.2012.08.028